A time-varying Kalman filter for low-acceleration attitude estimation☆

Álvaro Deibe Díaz [a,b,*], José A. Antón Nacimiento [c], Jesús Cardenal [c], Fernando López Peña [a,b]

[a] *Integrated Group for Engineering Research (GII), Vazquez Cabrera, 15403, Ferrol, Spain*
[b] *Ferrol Industrial Campus and Marine and Industrial Technologies Research Center (CITENI), Coruna, 15001, Spain*
[c] *Observatory for Design and Innovation in Mobility, Transportation and Automotion and Ferrol Industrial Campus, Vazquez Cabrera, Ferrol, 15403, Spain*

ARTICLE INFO

ABSTRACT

This work shows an attitude estimator (AE) based on a time-varying Kalman filter (TVKF) and adapted to those cases where a low-acceleration assumption can be applied. This filter is an extended version of a previously published time-varying Kalman filter attitude estimator (TVKAE). A comparative analysis of the accuracies of those two estimators is provided. The efficiencies of both filters are also compared with those of other published AEs. The results show that the new AE achieves the best overall performance, followed by the original one.

1. Introduction

Magnetic, angular rate, and gravity (MARG) sensors are widely used in attitude estimation through different sensor fusion implementations. The majority of those sensor fusion algorithms are either Kalman filters (KF) or complementary filters (CF). MARGs are devices made up of triads of magnetometers, accelerometers, and rate-gyros. The most common method of estimating orientation is by integrating the measured angular velocity data obtained from those gyroscopes. The initial conditions for integration are usually computed at rest by estimating the absolute orientation. For that, the local gravity vector is obtained from the accelerometer measurements, and the vector of the Earth's magnetic field from the magnetometer. However, MARG rate-gyro measurements are known to produce drift in the orientation estimation due to the integration of two components: a slowly changing bias instability and a higher frequency noise variable called angular random walk [1]. That drift is often corrected over time using the accelerometer and magnetometer measurements. However, accelerometers are sensitive to both gravity and acceleration, which is a consequence of the motion dynamics of the body to which the sensor is attached. Therefore, any accelerometer measurement is the sum of gravity and acceleration. Consequently, any assumption that acceleration measurements come only from gravity should lead to a loss of accuracy under dynamic conditions. However, there are many practical application cases in which the low acceleration assumption applies. In those cases, the time-averaged value of the accelerometer measurement is considered to be equal to gravity, and the approximation of neglecting the acceleration

due to motion works well. Examples of these applications range from industrial [2], medical [3,4], robotics [4,5], human motion and pose [6–9], or UAV navigation and control [9–11], among others. All these cases use the gravity value resulting from the direct measurement of accelerometers to estimate the attitude. In other words, in the above cited works the accelerometer signal is modeled as a noisy measurement of gravity.

The TVKAE presented in [12] is an AE that represents orientation and orientation changes using quaternions, models the dynamics of the process using time-varying matrices, and composes a specific state vector that is built up of measurable physical quantities, including acceleration. The original formulation of the Kalman filter [13] does not prevent the algorithm's matrices from varying with time. The Time-Varying Kalman Filter family (TVKF) takes advantage of this fact by using time-varying matrices to avoid some drawbacks of other non-linear approaches. For example, the evaluation of nonlinear functions, nonlinear transformation of the Gaussian Random Variable (GRV), Jacobian calculations in EKF type implementations, computational time overhead due to state–vector augmentation in sigma-point implementations, or cost of stochastic filters computation in $SO(3)$ in Birmingham Filters (BF) [14]. The TVKFs have been used in many applications, such as the estimation of the combustion torque on Diesel engines [15], predicting the remaining useful life of bearings [16], the dynamic tracking in frequency-scanning interferometry [17], or the fault detection in permanent magnet synchronous generators [18], among others. There are few examples of the application of TVKFs in attitude estimation,

such as the work of Bryson [19] or that of Gebre-Egziabher [20]. In most of the papers just mentioned, the matrices that vary with time are those of error covariance. Nevertheless, in the case of the TVKAE in [12], the Kalman gain matrix is also time-varying.

As mentioned before, the TVKAE that concerns the present work includes the acceleration within its state vector. That can be advantageous in some circumstances, as for estimating the attitude of bodies having dynamics where the mean of the accelerometer measurements does not coincide with gravity. However, this convenience is ineffective in cases of low acceleration where its time-averaged value is zero. That is often the case in many applications of interest, such as human body motion tracking and other applications of increasing interest in recent years. One of the objectives of this work is to present an estimator based on this TVKAE and adapt it for those cases of low acceleration. To do this, the initial formulation of that TVKAE is expanded by adding a new parameter helping to achieve that goal. Switching from the original formulation to the low-acceleration filter merely requires changing the value of this parameter from one to zero. In the case of implementing the new filter inside a MEMS device, it would be possible to simplify its internal matrices to reduce code size and increase computation speed. That is not necessary now because the comparisons use a high-level computing language and intend to be as simple and direct as possible.

The second objective of this work is to compare the behavior of the two TVKAE estimators, firstly with each other and then with some other EAs. For this, the two sets of experiments conducted in Deibe et al. [12] are used, in addition to an extensive comparison based on other published studies containing data, algorithms, and results for other EAs.

Numerous studies appear in the literature aimed at comparing and evaluating various sensor fusion algorithms for attitude determination, such as [21–25]. In general, the results published in these comparative studies can be quite different from each other. Those divergences arise from their different experimental conditions and the various settings on the parameters and operating conditions of the different algorithms. Among all these studies, the work by Caruso et al. [25] is one of the most complete and consistent. It also includes an extensive review of many of these works and presents an exhaustive summary of their results. In addition, the authors conduct a comprehensive experimental accuracy benchmarking of ten well-known and accepted attitude estimators, establish a normalized tuning method to obtain the optimal parameters of each filter, and provide a good amount of experimental data with the corresponding ground truth. These data and methodology belong to the realm of human body motion tracking and have been made accessible by their authors in public repositories. Consequently, the data, methods, and results presented in Caruso's work perfectly fit the purpose pursued. Therefore, they are going to be used in this work.

The work by Caruso et al. compares five Kalman and five complementary filters. The Kalman filters are those presented in [8] (SAB), [7] (LIG), [26] (VAK), [27] (GUO), and the MathWorks implementation of [28] (MKF). The complementary filters are those in [29] (MAH), [30] (MAD), [31] (VAC), [32] (SEL), and the MathWorks implementation of VAC with only two parameters (MCF). The experimental data necessary for the comparative evaluation of the precision of these ten AEs were recorded using three commercial MARG products when performing three maneuvers with them at three different rotational speeds. As ground truth, the orientation provided by a stereophotogrammetric (SP) camera system was used. The performance of the AEs was evaluated after the adjustment of optimal parameters, minimizing the root mean square value (RMS) of the orientation error when compared to the ground truth for each maneuver. Errors obtained using the default parameter values for each estimator were also calculated. This way, the impact of using generic and unadjusted parameter values for each experimental scenario is highlighted. Additionally, they accomplished a preliminary evaluation of computational efficiency in terms of CPU time spent by each AE. The authors have made the sensor fusion algorithms publicly available online, along with the complete dataset.

The Section 2 briefly describes the estimator, highlighting the relevant aspects for the development of this work and describing the modifications mentioned earlier in this introduction. In the Section 3, a comparison is first made between the two TVKAE estimators using the two experiments presented in [12]. Afterwards, Section 4 presents a comparative test of the accuracy of the two TVKAE and the other ten filters analyzed in the work of Caruso et al. [25]. Finally, the conclusions of this work are presented.

2. Filter algorithm

As stated above, the AE presented here is an improved version of the published TVKAE. This section briefly describes it. More details on that algorithm can be found in [12]. In addition, the necessary modifications in the formulation to adapt the filter to situations of negligible acceleration are introduced.

On each iteration, the algorithm first evaluates the new values of the time-varying matrices $\boldsymbol{\Phi}_k$ and $\mathbf{H}_k$. Then, it performs a *prediction* stage by following the formulation of the original KF [13]:

$$\hat{\mathbf{x}}_k^- = \boldsymbol{\Phi}_k \hat{\mathbf{x}}_{k-1}$$
$$\mathbf{P}_k^- = \boldsymbol{\Phi}_k \mathbf{P}_{k-1} \boldsymbol{\Phi}_k^T + \mathbf{Q}_k \tag{1}$$

and a *correction* stage:

$$\mathbf{K}_k = \mathbf{P}_k^- \mathbf{H}_k^T \left(\mathbf{H}_k \mathbf{P}_k^- \mathbf{H}_k^T + \mathbf{R}_k \right)^{-1}$$
$$\hat{\mathbf{x}}_k = \hat{\mathbf{x}}_k^- + \mathbf{K}_k \left(\mathbf{z}_k - \mathbf{H}_k \hat{\mathbf{x}}_k^- \right) \tag{2}$$
$$\mathbf{P}_k = \left(\mathbf{I} - \mathbf{K}_k \mathbf{H}_k \right) \mathbf{P}_k^-$$

The iteration completes with a normalization stage. This KF algorithm uses this prediction–correction scheme to recursively estimate $\mathbf{x}_k$. Matrices $\boldsymbol{\Phi}_k$ and $\mathbf{H}_k$ are time-varying and, consequently, $\mathbf{P}_k$ and $\mathbf{K}_k$. Matrices $\boldsymbol{\Phi}_k$ and $\mathbf{H}_k$ are computed at each time-step without using any nonlinear function.

In the following equations, a left superscript is used to note the reference system: $^b*$ denotes the *body* and $^e*$ the *earth* systems. The earth reference is a North-East-Down (NED) local coordinate system having the X axis ($\mathbf{e}_x$) pointing to the magnetic North.

The state vector $\mathbf{x}_k$ is made up of three vectorial quantities that define the dynamics of the tracked body: acceleration, orientation, and rotation. It can be expressed as:

$$^e\mathbf{x}_k = \begin{pmatrix} ^e\mathbf{a}_k & ^e\mathbf{q}_k & ^b\mathbf{v}_{r,k} \end{pmatrix}^T \tag{3}$$

where:

- $^e\mathbf{a}_k = \begin{pmatrix} a_x & a_y & a_z \end{pmatrix}^T$ is the acceleration vector,
- $^e\mathbf{q}_k = \begin{pmatrix} q_1 & q_2 & q_3 & q_4 \end{pmatrix}^T$ is a quaternion keeping track of the estimation of the body orientation, and
- $^b\mathbf{v}_{r,k} = \begin{pmatrix} v_x & v_y & v_z \end{pmatrix}^T$ is the vectorial part of the rotation quaternion $^b\mathbf{q}_r = \begin{pmatrix} \omega_0, & ^b\mathbf{v}_r \end{pmatrix}$ representing the orientation change in body coordinates between previous and actual state.

$^e\mathbf{q}_k$ and $^b\mathbf{q}_r$ are quaternions expressing orientation and orientation changes, so the algorithm must ensure that both remain unitary, for which the final normalization stage of the algorithm has been included.

The *measurement vector*, $\mathbf{z}_k$, is composed from the outputs of three triaxial sensors:

$$\mathbf{z}_k = \begin{pmatrix} ^b\mathbf{a}_k & ^b\mathbf{m}_k & ^b\boldsymbol{\omega}_k \end{pmatrix}^T \tag{4}$$

being

- $^b\mathbf{a}_k$ the outputs of an accelerometer,
- $^b\mathbf{m}_k$ the earth magnetic field measured with a magnetometer, and
- $^b\boldsymbol{\omega}_k$ the vectorial angular velocity from a *rate–gyro*.

Matrix $\boldsymbol{\Phi}$ in Eq. (1) is time-varying. It expresses the predicted change in the state vector, and it is built as block diagonal:

$$\boldsymbol{\Phi} = \text{diag}(\boldsymbol{\Phi}_{11}\ \boldsymbol{\Phi}_{22}\ \boldsymbol{\Phi}_{33}) \tag{5}$$

Block $\boldsymbol{\Phi}_{11}$ performs the predicted change in acceleration ${}^{e}\mathbf{a}_k$. In the original formulation the acceleration is assumed to remain constant in the prediction phase. In the present formulation a new parameter β has been introduced:

$$\boldsymbol{\Phi}_{11} = \beta\ \mathbf{I}_{3\times3} \ \Rightarrow \ {}^{e}\mathbf{a}_{k+1} \leftarrow \beta\ {}^{e}\mathbf{a}_k \tag{6}$$

This equation matches the original TVKAE filter formulation (TV1 from now on) only when β equals one. That is, when the acceleration remains constant at the prediction stage. The new formulation, with $\beta = 0$ (TV0), implements the low acceleration assumption. In this case, the $\boldsymbol{\Phi}_{11}$ block becomes null. The other two blocks of the $\boldsymbol{\Phi}$ matrix remain the same as in TV1.

The angular velocity is assumed to remain unchanged in the prediction stage. This dictates the expected change in orientation:

$$\boldsymbol{\Phi}_{22} \cdot {}^{e}\mathbf{q} = {}^{e}\mathbf{q} \otimes \begin{pmatrix} \omega_0 \\ {}^{b}\mathbf{v}_r \end{pmatrix} = (\omega_0 \cdot \mathbf{I}_{44} + \boldsymbol{\Omega}) \cdot {}^{e}\mathbf{q} \tag{7}$$

The use of quaternions ${}^{e}\mathbf{q}$ and ${}^{b}\mathbf{q}_r$ instead of, for example, rotation matrices or Euler angles, is crucial in these steps as it allows expressing orientation changes and rotations as vector–matrix products, thus preserving the original KF formulation:

$$\boldsymbol{\Phi}_{22} = \omega_0\mathbf{I}_{44} + \boldsymbol{\Omega} \ \Rightarrow \ {}^{e}\mathbf{q}_{k+1} \leftarrow \boldsymbol{\Phi}_{22} \cdot {}^{e}\mathbf{q}_k \tag{8}$$

$\boldsymbol{\Omega}$ changes with ${}^{b}\mathbf{v}_r$ (for more details, see [12]).

And finally, $\boldsymbol{\Phi}_{33}$ predicts the evolution of the angular velocity. During this stage, it is expected to remain constant, as explained, so:

$$\boldsymbol{\Phi}_{33} = \mathbf{I}_{3\times3} \ \Rightarrow \ {}^{b}\mathbf{v}_{r,k+1} \leftarrow {}^{b}\mathbf{v}_{r,k} \tag{9}$$

The covariance matrix $\mathbf{Q}$ models the process noise. It is composed of three blocks corresponding to the three components of the state vector, ${}^{e}\mathbf{a}_k$, ${}^{e}\mathbf{q}_k$, and ${}^{b}\mathbf{v}_{r,k}$. Thus:

$$\mathbf{Q} = \text{diag}(\mathbf{Q}_a\ \mathbf{Q}_q\ \mathbf{Q}_r) \tag{10}$$

The connection between state and measurement vectors is performed with the $\mathbf{H}$ matrix, which is upper triangular and has blocks that relate the different parts of both vectors:

$$\begin{pmatrix} {}^{b}\mathbf{a} \\ {}^{b}\mathbf{m} \\ {}^{b}\boldsymbol{\omega} \end{pmatrix} = \begin{pmatrix} \mathbf{H}_{11} & \mathbf{H}_{12} & \mathbf{0} \\ \mathbf{0} & \mathbf{H}_{22} & \mathbf{0} \\ \mathbf{0} & \mathbf{0} & \mathbf{H}_{33} \end{pmatrix} \cdot \begin{pmatrix} {}^{e}\mathbf{a} \\ {}^{e}\mathbf{q} \\ {}^{b}\mathbf{v}_r \end{pmatrix} \tag{11}$$

Matrices $\mathbf{H}_{11}$ and $\mathbf{H}_{12}$ depend on the orientation ${}^{e}\mathbf{q}$. The accelerometer output is related to the acceleration vector, the orientation quaternion, and the gravity vector:

$$\begin{pmatrix} 0 \\ {}^{b}\mathbf{a} \end{pmatrix} = {}^{e}\mathbf{q}^* \otimes \begin{pmatrix} 0 \\ {}^{e}\mathbf{a} \end{pmatrix} \otimes {}^{e}\mathbf{q} - g \cdot {}^{e}\mathbf{q}^* \otimes \begin{pmatrix} 0 \\ \mathbf{e}_z \end{pmatrix} \otimes {}^{e}\mathbf{q} \tag{12}$$

The value of the gravity vector is estimated at the start of each test, and is expected to be invariant.

The use of quaternions to express orientation and rotation allows to write Eq. (12) as matrix–vector and matrix–quaternion products:

$$\mathbf{b}\mathbf{a} = \mathbf{H}_{11} \cdot {}^{e}\mathbf{a} + \mathbf{H}_{12} \cdot {}^{e}\mathbf{q} \tag{13}$$

Note that making $\beta = 0$ in the prediction phase (Eq. (6)) nullifies the value of the predicted acceleration ${}^{e}\mathbf{a}$, thus rendering the first term of the right-hand side of Eq. (12) null. That is, if $\beta = 0$, Eq. (12) become:

$$\begin{pmatrix} 0 \\ {}^{b}\mathbf{a} \end{pmatrix} = -g \cdot {}^{e}\mathbf{q}^* \otimes \begin{pmatrix} 0 \\ \mathbf{e}_z \end{pmatrix} \otimes {}^{e}\mathbf{q} = -g \cdot \begin{pmatrix} 0 \\ {}^{b}\mathbf{e}_z \end{pmatrix} \tag{14}$$

In this expression, it becomes clear that when $\beta = 0$ accelerometer measurements are directly related to the gravity vector, and the acceleration is neglected. As has been said, in this case, the accelerometer output can be considered a noisy measurement of the gravity field.
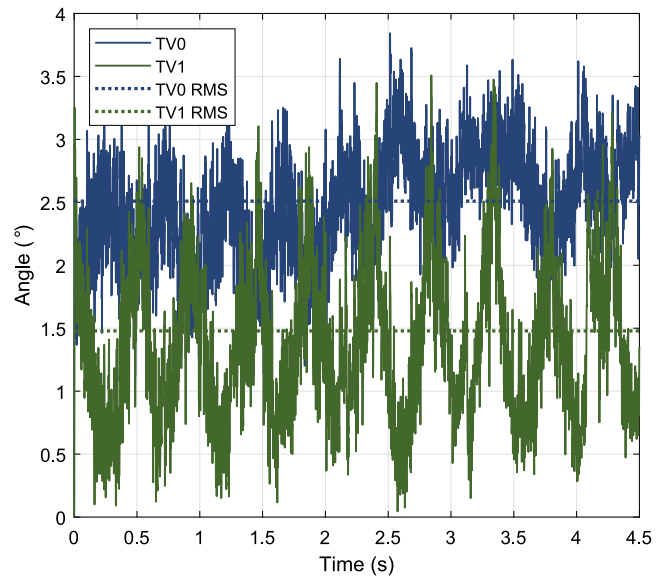

Fig. 1. Absolute orientation error for TV0 and TV1 and RMS values.

The magnetometer output is estimated by expressing the Earth's magnetic field in body coordinates. Thus, by using the orientation quaternion:

$$\mathbf{b}\mathbf{m} = h \cdot {}^{e}\mathbf{q}^* \otimes \left(\sin\alpha \begin{pmatrix} 0 \\ \mathbf{e}_x \end{pmatrix} + \cos\alpha \begin{pmatrix} 0 \\ \mathbf{e}_z \end{pmatrix} \right) \otimes {}^{e}\mathbf{q} \tag{15}$$

As explained, $\mathbf{e}_x$ points in the direction of the magnetic north. Therefore, the vector of the earth magnetic field lies in the XZ plane. The angle α is measured between the magnetic field vector and $\mathbf{e}_x$, while h measures the strength of the magnetic field. Again, the use of quaternions makes it possible to write equation (15) as a matrix–vector product:

$$\mathbf{b}\mathbf{m} = \mathbf{H}_{22} \cdot {}^{e}\mathbf{q} \tag{16}$$

The angular velocity of the tracked body, and thus the change of orientation in each iteration, which is expressed with quaternion ${}^{b}\mathbf{q}_r$, is directly related to the rate–gyro readings. Only ${}^{b}\mathbf{v}_r$, the vectorial part of ${}^{b}\mathbf{q}_r$, is needed to estimate this change in orientation:

$$\mathbf{b}\boldsymbol{\omega} = \mathbf{H}_{33}{}^{b}\mathbf{v}_r \tag{17}$$

where:

$$\mathbf{H}_{33} = \frac{2}{\Delta t}\mathbf{I}_{3\times3} \tag{18}$$

The MATLAB code of this filter has been made publicly available [33].

3. Proof of concept analysis

In the article presenting TV1 [12], the results of a synthetic and a real test case were discussed and used as proof of concept for the estimator. These tests are used here to compare the performance of both filters, TV0 and TV1.

In the first case, TV0 and TV1 are fed with inertial data coming from the numerical simulation of a mechanical system: the simulation is based on a planar double pendulum subjected to high angular speeds and accelerations. The maneuver is numerically solved to compute the main static and dynamic magnitudes.

In the real life test case, a MARG attached to a solid is used to sense its movement during a maneuver.
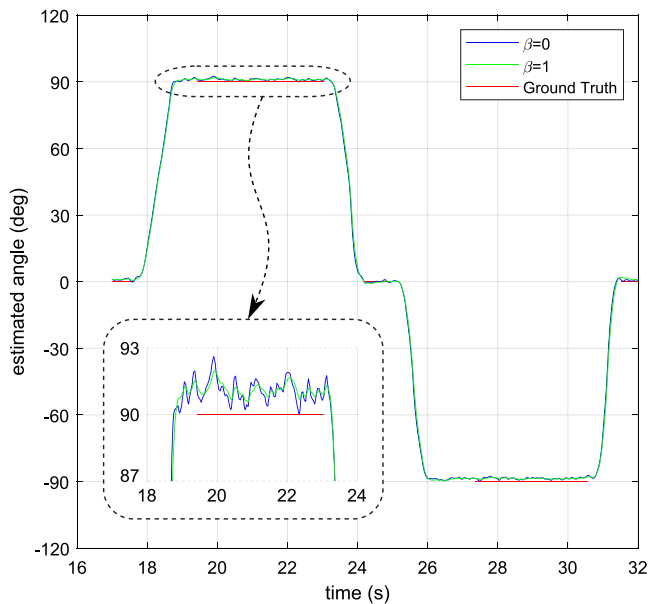
Fig. 2. Estimated orientation angle for TV0 and TV1 in a decoupled turn on Y axis.

Table 1
RMS error for TV0 and TV1 in decoupled turns around $X, Y,$ and Z axes.

	X	Y	Z	Total
$\beta = 0$	3.2°	3.5°	4.4°	3.3°
$\beta = 1$	4.3°	4.0°	6.3°	4.3°

3.1. Double pendulum

Consider a double compound pendulum that has its bars linked with revolute joints. The axis of both joints are horizontal and parallel, so the movement of both bars is in the same vertical plane. The system is supposed to be ideal and subjected only to gravity forces. The governing ODE numerical problem is solved, and the solution is taken as ground truth. Synthetic measurements from a virtual MARG sensor attached to the second link are then computed numerically. The MARG sensor does not have the information that the movement is planar, so the measurements are made as if it was three-dimensional. More details about this synthetic test set-up can be found in [12].

The experiment begins with both bars in a horizontal position, disengaged, and left to evolve freely under the action of gravity. Both bars are 2 m long and weigh in at 1 kg. The first bar is motionless at the start of the maneuver; the initial rotational speed of the second bar is 20 rad s^{-1}. This value is chosen to be high enough to show the effects of $\beta = 0$ in an environment of high accelerations. The ODE system is integrated by means of an implicit second order method with a time step size of 1 ms. The first 4.5 s of the evolutions of the second bar are then sampled at 1 ms with a virtual IMU attached to it. Finally, white, zero–mean, Gaussian noises are added to the sampled signals. The STD of these noises match those of the real IMU used in the second experiment.

These synthetic samples feed both attitude estimators, TV0 and TV1. The estimated orientation quaternion at each time step is compared against the ground truth. The RMS value of the angular orientation error is computed for both estimators, leading to 2.51° for TV0, and 1.48° for TV1. That is, TV0 shows an increment in the error of the estimated orientation angle of 70% compared to that of TV1. Fig. 1 shows the absolute difference between ground truth and estimated orientation angle in both cases (TV0 and TV1), and it also depicts the RMS value for both versions of the estimator.

That is the expected behavior in an experiment under high acceleration, jerk, and having a mean of acceleration that does not match the gravity vector. In this kind of maneuver, assuming $\beta = 0$ and thus neglecting acceleration, a sub-optimal estimator outcome is expected. That is also the case for any attitude estimator that treats accelerometer signals as a noisy gravity measurement. The original estimator, TV1 (with $\beta = 1$), is better suited to this scenario.

3.2. Consecutive independent turns

The second experiment intends to show the ability to track actual body movements. Several independent and sequential turning maneuvers are performed on a solid box equipped with a MARG sensor. The evolution of acceleration, angular velocities, and the magnetic field over time is measured. The ground truth only exists during the times between turns, in which the solid remains at rest, supported by a fixed stand. While moving, the only attitude reference is the one provided by the estimators. Hardware specifications and methods used in this test are detailed in the article by Deibe et al. [12].

Three independent maneuvers have been carried out in this test. Each consists of three consecutive turns around one of the three coordinate axes, with 1 s rest intervals between them. It starts with a quarter turn in the positive direction of the axis, followed by a half turn in the opposite direction and, again, a positive quarter turn, leaving the solid in the initial orientation. The turning rate is of around $\pi/2$ rad s^{-1}. The maneuver is successively repeated by rotating around each of the reference axes. Between two consecutive maneuvers, there is an interval of 5 s at rest. As the maneuvers are by hand, the specified angles, speed, and times can only be taken as a guide. However, during the rest intervals, the body remains still, rigidly attached to a support that guarantees its orientation. These rest intervals are used as ground truth, starting when the internal IMU stops registering vibrations until motion is detected again.

Fig. 2 represents one turning maneuver around the Y axis. The turning movements around the other two axes are similar to this. It can be seen that TV0 and TV1 perform very similarly. The red line represents the ground truth. As stated before, it only exists while the body is at absolute rest. The accuracy of the ground truth is affected by different manufacturing tolerances: the case, the circuit board supports, the circuit itself, and the internal alignment of the MEMS device. The accuracy is estimated to be within ±1°. Considering the attitude estimation error as the difference between the estimation and the ground truth, the resulting RMS error can be seen in Table 1, for each of the rotations around $X, Y,$ and Z, as well as for the whole maneuver. As expected, TV0 performs better than TV1 in this type of maneuver.

To compute the attitude estimation error, the difference between the estimated orientation quaternion and the ground truth quaternion is computed at each time-step as a product of the first by the conjugate of the second. From the resulting rotation quaternion, the angle is extracted and converted to degrees. Then the RMS value of all those error angles is computed. This method is the same used in [25], and will be used throughout Section 4.

4. Comparative analysis

As indicated above, the present experimental analysis on the accuracy of the TV0 and TV1 estimators uses the information and data[1] published in the studies by Caruso et al. [25,34]. Both algorithms are applied to estimate the attitude using the data of those experimental scenarios. The results are tested against the published ground truth to assess their accuracy and compare it with those published for the other ten algorithms. The methodology used to evaluate the precision of the other ten AEs is thoroughly followed to obtain those of TV0 and TV1.

---

[1] Version v4 of data files has been used for the present work.

Table 2
Optimum parameters at minimum error values for each speed/hardware combination for TV0.

Device	XSense			APDM			Shimmer		
Maneuver	Slow	Medium	Fast	Slow	Medium	Fast	Slow	Medium	Fast
Error [°]	1.3	1.6	1.9	3.2	3.2	4.6	2.9	2.9	5.1
σ_a [m s^{-2}]	5.1e−03	1.4e−02	1.6e−03	1.2e+00	5.1e+00	7.9e−10	6.5e−02	2.6e−10	4.8e−02
σ_q	6.1e−07	8.9e−07	2.7e−08	3.8e−04	4.7e−05	1.2e−07	1.3e−05	9.7e−08	9.8e−06

4.1. Experimental data

In the study by Caruso et al. three commercial MARG devices were used, namely Xsens, APDM, and Shimmer [25]. Two units of each were mounted on a flat board and aligned with an alignment error of fewer than 0.2 degrees. That board was marked with eight reflective spherical markers to provide orientation references whose trajectories were acquired by an SP system having 12 infrared cameras. Singular value decomposition was used to estimate the orientation over time [35]. The resulting gold standard orientation, or ground truth, has an accuracy of 0.5 degrees and was expressed using a quaternion.

The ground truth and the data from all the MARGs were stored in three available dynamic recordings, corresponding to three maneuvers with three different angular velocity conditions. Those are called slow, medium, and fast. The board was moved by hand, covering all three rotational degrees of freedom in all three maneuvers while performing single and triaxial rotations. Then, the RMS of the rotational speed was numerically obtained, yielding 120° s^{-1} (slow), 260° s^{-1} (medium), and 380° s^{-1} (fast). Given the specifications provided and the rotation speeds indicated, the denominations slow, medium, and fast make sense when in the realm of human body motion tracking. Consequently, for all three maneuvers using the low acceleration assumption is still appropriate. All AEs in the comparison make use of this assumption, but TV1.

The results obtained when evaluating the performance of these ten algorithms have also been made available. These published results are used directly in the present work to compare them with those obtained for TV0 and TV1. The methodology used to assess the accuracy of the other ten AEs is also followed to evaluate those two. The first step is to identify the optimal parameter values. That is, the values that provide minimum errors for each of those two estimators in the nine possible combinations of maneuver speeds and MARG hardware.

4.2. Parameter optimization

Any AE requires adjusting some parameters to work accurately. This setting not only depends on the estimator but also on the type of maneuver performed and the MARG device used. Optimizing the parameters will provide the minimum RMS orientation error in each scenario. In the reference work [25], the maximum number of parameters to be optimized was restricted to only two for each AE. Optimization was performed for each of the nine experimental scenarios using actual SP attitude data as ground truth.

In the case of the filter presented in Section 2, there are three relevant parameters that can be adjusted, the standard deviations σ_a, σ_q, and σ_{qr} of acceleration $^e\mathbf{a}$, orientation quaternion $^e\mathbf{q}$, and rotation quaternion $^e\mathbf{q}_r$, respectively. A preliminary sensitivity study has shown that the most relevant parameters are the standard deviations σ_a and σ_q. Therefore, these two parameters are chosen to be optimized in each experimental scenario. All other parameters are set to default values.

The first step toward choosing those two parameters is to find an optimal tuning setting for each experimental scenario. That is, determining which pair of values of these two parameters minimize the RMS orientation error for each case. That allows evaluating what estimator tuning yields the best performance. Table 2 presents the optimal values of σ_a and σ_q leading to the best overall performance of TV0 in the nine experimental scenarios. The table also shows the value of that error for

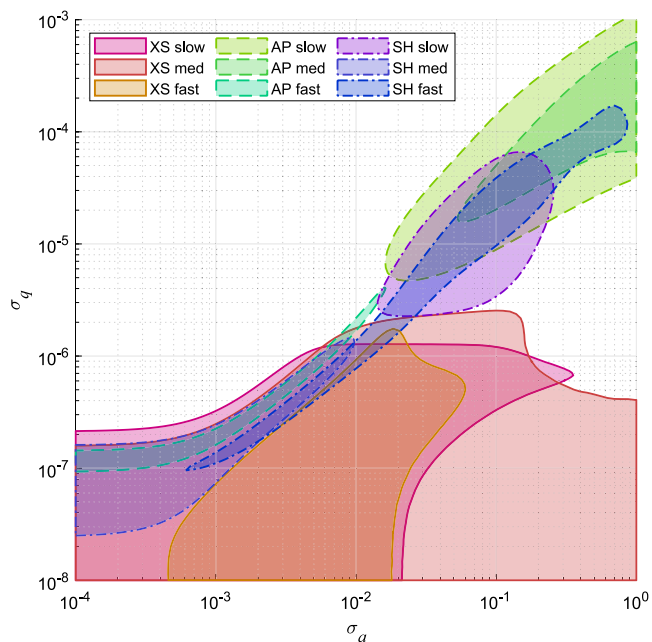**Fig. 3.** TV0 optimal regions for the nine experimental scenarios.

each case. The values of σ_a and σ_q presented in the table are those used in the attitude estimation calculations in each scenario.

An optimal region is defined from the optimal values of the two chosen parameters. It covers the area in the two-parameter plane for which the RMS orientation error is less than the lowest error plus 0.5 degrees, which corresponds to the uncertainty of the SP providing the ground truth. Fig. 3 represents the nine optimal regions for TV0. Optimal regions are represented with a different color for each scenario. Those regions have been calculated with an accuracy of ±0.001°.

In that figure there is no common intersection between all optimal regions. Which is also the case for all other algorithms but MKF [25]. All this confirms that there are no set of parameters that optimizes the orientation error for all scenarios. After MKF, TV0 is the one that presents a better grouping and intersection between the nine optimal regions.

4.3. Results and discussion of the accuracy comparison test

After identifying the optimal values of the two parameters corresponding to each of the nine experimental scenarios for TV0 and TV1, the absolute errors of attitude estimation have been calculated. These calculations have followed the same procedure used by Caruso et al. [25] to compute the orientation estimation error. The results are compared in Fig. 4 with those published there for the other ten AEs.

As expected, TV0 gives better results than TV1. That is the case in all experimental scenarios except for medium and fast APDM maneuvers, where they behave almost similarly. Notably, TV0 is the algorithm with the highest accuracy. It performs best in all the comparisons, except in the medium maneuver with APDM, for which it acts worse than TV1. Also, it matches VAK using Xsens hardware in the slow and

Table 3
Mean and STD error for each algorithm.

Type	TVK		Kalman					Complementary				
AE	TV0	TV1	SAB	LIG	VAK	GUO	MKF	MAH	MAD	VAC	SEL	MCF
Mean error [°]	3.0	3.6	4.8	3.8	4.5	5.8	6.0	4.6	4.8	6.6	5.3	7.1
STD error [°]	1.3	1.5	2.4	1.4	2.8	3.7	2.2	2.1	2.2	2.9	2.4	2.9
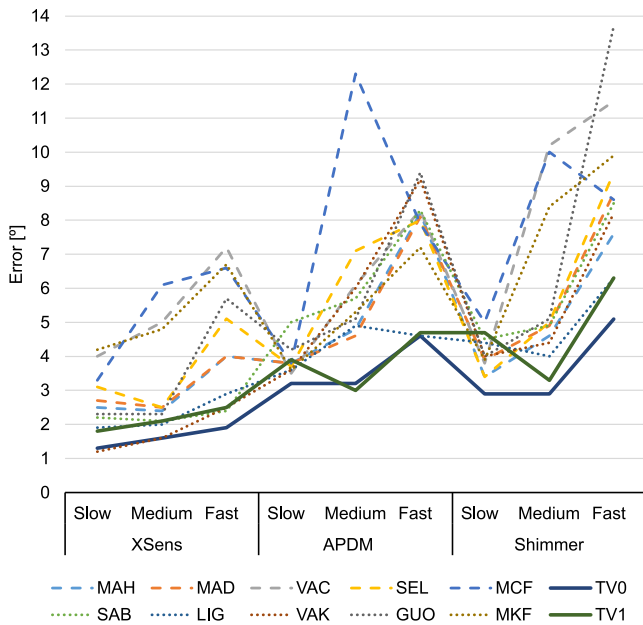
Fig. 4. Comparison of the performance of all AE algorithms.

Fig. 5. Box plot for the error of TVKAE, Kalman filter and complementary filter algorithms.

medium maneuvers and LIG and TV1 in the fast ones, using APDM and Shimmer, respectively. It is also worth noting that TV1 is among the best performers, despite being the only one not planned for low acceleration.

The results of Fig. 4 are collected in Table 3. The showed mean and STD values of the errors for each algorithm are estimated combining those coming from every hardware–speed combination of the experiment. This table complements the one published in Caruso [25], adding the results for TV0 and TV1. As can be seen in Table 3, TV0 is the estimator with the lowest mean error, followed by TV1. Also, TV1 STD is lower than all but LIG, and TV0 has the lowest STD of all algorithms.

Fig. 5 shows box plots for the RMS errors (in degrees) of each algorithm over the nine different speed/ hardware combinations. Again, although TV1 is not well suited for this kind of manoeuvres, it is better than all algorithms but LIG. TV0 shows the best performance of all algorithms.

4.4. Computational efficiency

An analysis of the computational efficiency of the filters tested in this article is performed here by measuring the time each of the filters needs to execute the complete simulation of one maneuver. A full simulation comprises all tasks, from reading data to final error estimation operations. The assessment compares the average time of each algorithm to finish four complete runs of the slow maneuver. For all filters except TVKs, the Matlab code provided by Caruso et al. [25], as found in their repository, is used without any alteration. For the TVKs, the Matlab code published in the repository [33], is used. Since in this code there is no difference in terms of computation time when a specific value of the β parameter is chosen in the TVK, the run was performed only for $\beta = 0$ (TV0). The execution of each code has been
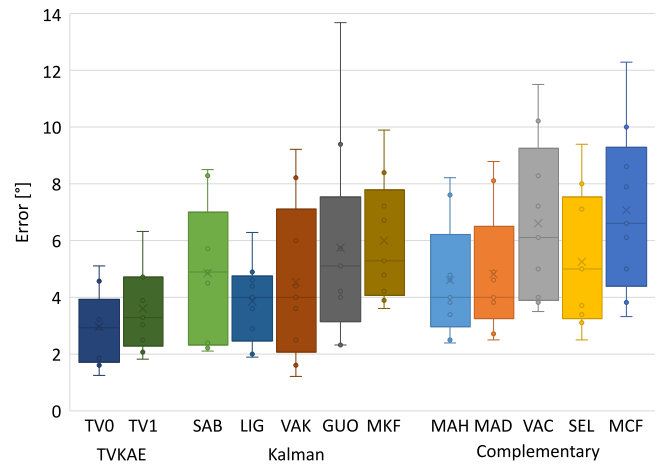
done on an Intel Core i7-6th Gen @ 4.00 GHz Microsoft Windows 10 computer. Table 4 shows the execution time values, both in absolute terms and normalized with those required by TV0.

These results cannot be considered a precise measure of efficiency due to the heterogeneity in the implementations and fundamentals of each algorithm; and because there was no tuning effort to optimize the code. Nevertheless, they can be taken as a rough comparison of efficiency. With this caution, the performance of TVK is remarkable, as the results show that it is the best Kalman-based AE but GUO. But this algorithm is explicitly designed by its authors to work fast, although it is not very precise (see Fig. 4). In general, complementary filters are faster than Kalman filters due to their mathematical implementation. Therefore, it is also worth noting that the TVKF performs better than two of the CFs, even though the MATLAB implementation of TVK is not optimized by the authors to run fast.

5. Conclusion

This work presents a TVKF-based attitude estimator. The algorithm is an extended version of the AE by Deibe et al. [12] that adapts better to negligible acceleration cases. The extended version of the filter is developed by including a new weighting parameter. When this weight is unity, the filter retains its original algorithm. Setting it to zero leads to a version adapted to low acceleration. Additionally, some peculiarities have been discussed concerning the handling of acceleration and gravity when this parameter is zero. The MATLAB code of the resulting TVKF has been made publicly available [33].

The accuracy of the two TVKAEs is first compared using two published experiments. The first is a simulation in which the solution of the ODEs that govern the movement of a compound pendulum is the ground truth. In this case, the accelerometer measurement does not match gravity, and TV1 performs 69.7% better than TV0. The second experiment follows the motion of a solid body rotated by hand. In this case, the average value of the accelerometer measurements does coincide with gravity, and it is TV0 that performs 23% better than TV1. Then, a comprehensive comparative analysis is made with the published results of other estimators when applied to cases of low

Table 4
Execution time for every algorithm.

Time	TVK	Kalman						Complementary				
[s]		SAB	LIG	VAK	GUO	MKF		MAH	MAD	VAC	SEL	MCF
Absolute	1.93	2.20	19.30	2.70	0.92	16.68		0.94	1.02	1.09	2.67	21.24
Relative	1.00	1.14	10.00	1.40	0.48	8.65		0.49	0.53	0.56	1.38	11.01

acceleration. This comparative analysis uses a standard benchmark corresponding to this field and its data. These have been published together with the codes and results obtained with ten estimators: five Kalman filters and five complementary filters. That comparison shows that the new filter works better than the original. In addition, it has the best accuracy and STD among the twelve filters used in the assessment. Remarkably, the original version of the AE ranks second despite being the only one not devised for low accelerations.

A rough analysis of the computational efficiency is also presented. This analysis uses the published MATLAB code of all the mentioned AEs. For this study, the structure of TV0 has been kept identical to that of TV1. Therefore, the execution of both versions of TVKAE requires the same number of operations. Thus, in this computational efficiency study, only one version is used. It has been noted that the code of one of the KFs is optimized to improve computational speed. All the others, including TVKAE, have not been optimized in this regard. The analysis shows that the TVK is quicker than all the KFs, except the optimized one, and it is also faster than two of the CF.

CRediT authorship contribution statement

Álvaro Deibe Díaz: Conceptualization, Methodology, Software, Writing – original draft, Writing – review & editing. **José A. Antón Nacimiento:** Software, Validation, Formal analysis, Visualization. **Jesús Cardenal:** Software, Validation, Formal analysis, Visualization, Writing – review & editing. **Fernando López Peña:** Supervision, Data curation, Writing – original draft, Writing – review & editing.

Declaration of competing interest

The authors declare that they have no known competing financial interests or personal relationships that could have appeared to influence the work reported in this paper.

Data availability

The MATLAB code of the proposed algorithm has been made publicly available [33].

Acknowledgments

References

[1] Oliver J. Woodman, An Introduction To Inertial Navigation, Technical Report 696, University of Cambridge, Computer Laboratory, 2007.

[2] Weijie Zhang, Jun Xiao, HePing Chen, YuMing Zhang, Measurement of three-dimensional welding torch orientation for manual arc welding process, Meas. Sci. Technol. 25 (3) (2014) 035010, http://dx.doi.org/10.1088/0957-0233/25/3/035010.

[3] Nima Enayati, Elena De Momi, Giancarlo Ferrigno, A quaternion-based unscented Kalman filter for robust optical/inertial motion tracking in computer-assisted surgery, IEEE Trans. Instrum. Meas. 64 (8) (2015) 2291–2301, http://dx.doi.org/10.1109/TIM.2015.2390832.

[4] M.H. Korayem, M.A. Madihi, V. Vahidifar, Controlling surgical robot arm using leap motion controller with Kalman filter, Measurement (ISSN: 0263-2241) 178 (2021) 109372, http://dx.doi.org/10.1016/j.measurement.2021.109372.

[5] Alexander McGregor, Gordon Dobie, Neil R. Pearson, Charles N. MacLeod, Anthony Gachagan, Determining position and orientation of a 3-wheel robot on a pipe using an accelerometer, IEEE Sens. J. (ISSN: 1530-437X) 20 (9) (2020) 5061–5071, http://dx.doi.org/10.1109/JSEN.2020.2964619, (2379) 1558-1748-9153.

[6] Nasim Hajati, Amin Rezaeizadeh, A wearable pedestrian localization and gait identification system using Kalman filtered inertial data, IEEE Trans. Instrum. Meas. 70 (2021) 1–8, http://dx.doi.org/10.1109/TIM.2021.3073440.

[7] Gabriele Ligorio, Angelo M. Sabatini, A novel Kalman filter for human motion tracking with an inertial-based dynamic inclinometer, IEEE Trans. Biomed. Eng. 62 (8) (2015) 2033–2043, http://dx.doi.org/10.1109/TBME.2015.2411431.

[8] Angelo Maria Sabatini, Estimating three-dimensional orientation of human body parts by inertial/magnetic sensing, Sensors (ISSN: 1424-8220) 11 (2) (2011) 1489–1525, http://dx.doi.org/10.3390/s110201489.

[9] Zeyang Dai, Lei Jing, Lightweight extended kalman filter for marg sensors attitude estimation, IEEE Sens. J. 21 (13) (2021) 14749–14758, http://dx.doi.org/10.1109/JSEN.2021.3072887.

[10] Chingiz Hajiyev, Demet Cilden-Guler, Ulviye Hacizade, Two-stage Kalman filter for fault tolerant estimation of wind speed and uav flight parameters, Meas. Sci. Rev. 20 (1) (2020) 35–42, http://dx.doi.org/10.2478/msr-2020-0005.

[11] Dingjie Wang, Yi Dong, Qingsong Li, Jie Wu, Yule Wen, Estimation of small uav position and attitude with reliable in-flight initial alignment for mems inertial sensors, Metrol. Meas. Syst. 25 (3) (2018) 603–616, http://dx.doi.org/10.24425/123904.

[12] Álvaro Deibe, José Augusto Antón Nacimiento, Jesús Cardenal, Fernando López Peña, A Kalman filter for nonlinear attitude estimation using time variable matrices and quaternions, Sensors 20 (23) (2020) 6731, http://dx.doi.org/10.3390/s20236731.

[13] Rudolph Emil Kalman, A new approach to linear filtering and prediction problems, Trans. ASME (ISSN: 0021-9223) 82 (Series D) (1960) 35–45, http://dx.doi.org/10.1115/1.3662552.

[14] Weixin Wang, Peter G. Adamczyk, Comparison of bingham filter and extended kalman filter in imu attitude estimation, IEEE Sens. J. 19 (19) (2019) 8845–8854, http://dx.doi.org/10.1109/JSEN.2019.2922321.

[15] Jonathan Chauvin, Gilles Corde, Philippe Moulin, Michel Castagne, N. Petit, Pierre Rouchon, Real-time combustion torque estimation on a diesel engine test bench using time-varying Kalman filtering, in: Proceedings of the 43rd IEEE Conference on Decision and Control (CDC) (IEEE Cat. No. 04CH37601), Volume 2, ISBN: 0-7803-8682-5, 2004, pp. 1688–1694, http://dx.doi.org/10.1109/CDC.2004.1430287.

[16] Lingli Cui, Xin Wang, Huaqing Wang, Jianfeng Ma, Research on remaining useful life prediction of rolling element bearings based on time-varying Kalman filter, IEEE Trans. Instrum. Meas. 69 (6) (2020) 2858–2867, http://dx.doi.org/10.1109/TIM.2019.2924509.

[17] Xingyu Jia, Zhigang Liu, Long Tao, Zhongwen Deng, Frequency-scanning interferometry using a time-varying Kalman filter for dynamic tracking measurements, Opt. Express 25 (21) (2017) 25782–25796, http://dx.doi.org/10.1364/OE.25.025782.

[18] Karim Beddek, Adel Merabet, Mohamed Kesraoui, Aman A. Tanvir, Rachid Beguenane, Signal-based sensor fault detection and isolation for PMSG in wind energy conversion systems, IEEE Trans. Instrum. Meas. 66 (9) (2017) 2403–2412, http://dx.doi.org/10.1109/TIM.2017.2700138.

[19] Arthur E. Bryson, Kalman filter divergence and aircraft motion estimators, J. Guid. Control 1 (1) (1978) 71–79, http://dx.doi.org/10.2514/3.55745.

[20] D. Gebre-Egziabher, G.H. Elkaim, J.D. Powell, B.W. Parkinson, A gyro-free quaternion-based attitude determination system suitable for implementation using low cost sensors, in: IEEE 2000. Position Location and Navigation Symposium (Cat. No. 00CH37062), 2000, pp. 185–192, http://dx.doi.org/10.1109/PLANS.2000.838301.

[21] Alexander David Young, Comparison of orientation filter algorithms for realtime wireless inertial posture tracking, in: 2009 Sixth International Workshop on Wearable and Implantable Body Sensor Networks, IEEE, 2009, pp. 59–64, http://dx.doi.org/10.1109/BSN.2009.25.

[22] Panos Marantos, Yannis Koveos, Kostas J. Kyriakopoulos, Uav state estimation using adaptive complementary filters, IEEE Trans. Control Syst. Technol. 24 (4) (2016) 1214–1226, http://dx.doi.org/10.1109/TCST.2015.2480012.

[23] Elena Bergamini, Gabriele Ligorio, Aurora Summa, Giuseppe Vannozzi, Aurelio Cappozzo, Angelo Maria Sabatini, Estimating orientation using magnetic and inertial sensors and different sensor fusion approaches: Accuracy assessment in manual and locomotion tasks, Sensors (ISSN: 1424-8220) 14 (10) (2014) 18625–18649, http://dx.doi.org/10.3390/s141018625.

[24] Milad Nazarahari, Hossein Rouhani, 40 Years of sensor fusion for orientation tracking via magnetic and inertial measurement units: Methods, lessons learned, and future challenges, Inf. Fusion (ISSN: 1566-2535) 68 (2021) 67–84, http://dx.doi.org/10.1016/j.inffus.2020.10.018.

[25] Marco Caruso, Angelo Maria Sabatini, Daniel Laidig, Thomas Seel, Marco Knaflitz, Ugo Della Croce, Andrea Cereatti, Analysis of the accuracy of ten algorithms for orientation estimation using inertial and magnetic sensing under optimal conditions: One size does not fit all, Sensors (ISSN: 1424-8220) 21 (7) (2021) 2543, http://dx.doi.org/10.3390/s21072543.

[26] Roberto G. Valenti, Ivan Dryanovski, Jizhong Xiao, A linear Kalman filter for marg orientation estimation using the algebraic quaternion algorithm, IEEE Trans. Instrum. Meas. 65 (2) (2016) 467–481, http://dx.doi.org/10.1109/TIM.2015.2498998.

[27] Siwen Guo, Jin Wu, Zuocai Wang, Jide Qian, Novel MARG-sensor orientation estimation algorithm using fast Kalman filter, J. Sensors (ISSN: 1687-725X) 2017 (2017) 8542153, http://dx.doi.org/10.1155/2017/8542153.

[28] Daniel Roetenberg, Henk Luinge, Christian T.M. Baten, Peter H. Veltink, Compensation of magnetic disturbances improves inertial and magnetic sensing of human body segment orientation, IEEE Trans. Neural Syst. Rehabil. Eng. 13 (2005) 395–405, http://dx.doi.org/10.1109/TNSRE.2005.847353.

[29] Robert Mahony, Tarek Hamel, Jean-Michel Pflimlin, Nonlinear complementary filters on the special orthogonal group, IEEE Trans. Automat. Control 53 (5) (2008) 1203–1218, http://dx.doi.org/10.1109/TAC.2008.923738.

[30] Sebastian O.H. Madgwick, Andrew J.L. Harrison, Ravi Vaidyanathan, Estimation of imu and marg orientation using a gradient descent algorithm, in: 2011 IEEE International Conference on Rehabilitation Robotics, 2011, pp. 1–7, http://dx.doi.org/10.1109/ICORR.2011.5975346.

[31] Roberto G. Valenti, Ivan Dryanovski, Jizhong Xiao, Keeping a good attitude: A quaternion-based orientation filter for imus and margs, Sensors (ISSN: 1424-8220) 15 (8) (2015) 19302–19330, http://dx.doi.org/10.3390/s150819302.

[32] Thomas Seel, Stefan Ruppin, Eliminating the effect of magnetic disturbances on the inclination estimates of inertial sensors, IFAC-PapersOnLine (ISSN: 2405-8963) 50 (1) (2017) 8798–8803, http://dx.doi.org/10.1016/j.ifacol.2017.08.1534.

[33] Álvaro Deibe, José Augusto Antón Nacimiento, Jesús Cardenal, Fernando López Peña, Time-Varying Kalman Attitude Estimator (TVKAE), GitHub repository (2023) https://github.com/GII/TVKAE.

[34] Marco Caruso, Angelo Maria Sabatini, Marco Knaflitz, Marco Gazzoni, Ugo Della Croce, Andrea Cereatti, Orientation estimation through magneto-inertial sensor fusion: A heuristic approach for suboptimal parameters tuning, IEEE Sens. J. 21 (3) (2021) 3408–3419, http://dx.doi.org/10.1109/JSEN.2020.3024806.

[35] A. Cappozzo, A. Cappello, U.D. Croce, F. Pensalfini, Surface-marker cluster design criteria for 3-d bone movement reconstruction, IEEE Trans. Biomed. Eng. (ISSN: 1558-2531) 44 (12) (1997) 1165–1174, http://dx.doi.org/10.1109/10.649988.